Controlling polymer morphology in blade-coated all-polymer solar cells

Sebastian A. Schneider[1,3], Kevin L. Gu[2], Hongping Yan[2,3], Maged Abdelsamie[3,4], Zhenan Bao[2] and Michael F. Toney[5*]

[1] Department of Chemistry, Stanford University, Stanford, CA 94305, USA.
[2] Department of Chemical Engineering, Stanford University, Stanford, CA 94305, USA.
[3] Stanford Synchrotron Radiation Lightsource, SLAC National Accelerator Laboratory, Menlo Park, CA 94025, USA.
[4] Molecular Foundry, Lawrence Berkeley National Laboratory, Berkeley, CA 94720, USA.
[5] Department of Chemical and Biological Engineering, University of Colorado, Boulder, CO 80309, USA.

Abstract:

Translating all-polymer solar cells from spin-coating to scalable roll-to-roll (R2R) compatible fabrication techniques is a critical step towards the application of organic photovoltaics (OPVs) at scale. Techniques to control polymer crystallization and phase separation during solution printing are essential to achieve high performance printed organic solar cells. Here we demonstrate a novel solvent additive approach employing trace amounts of phthalates as additives to control polymer crystallinity and suppress unfavorable phase separation in a representative PTB7-Th/P(NDI2OD-2T) all-polymer solar cell. The best performing additive increased the blade-coated device performance from 2.09% to 4.50% power conversion efficiency, an over two-fold improvement, mitigating the loss in performance that is typically observed during process transfer from spin-coating to blade-coating. It is suggested that the improved device performance stems from a finer polymer phase-separation size and overall improved active layer morphology, evidenced by device characterization data and indirectly supported by grazing incidence wide angle X-ray scattering

(GIWAXS) analyses. Real time X-ray diffraction measurements during blade-coating provide mechanistic insight and suggest that the dioctyl phthalate additive may act as compatibilizer, reducing the demixing of donor and acceptor polymer during film formation, enabling a smaller phase-separation and improved performance. The structural diversity of the class of phthalate additives makes this simple yet effective concept promising for translating other all-polymer material systems to blade-coating and other scalable printing techniques.

1. Introduction

Organic photovoltaics (OPVs) based on polymeric semiconductors are attractive candidates for lightweight and low-cost renewable energy applications with a flexible form factor. The power conversion efficiency (PCE) of single-junction OPVs have recently surpassed 18%[1] and 15%[2,3] for polymer small-molecule and all-polymer systems, respectively. All-polymer OPVs featuring a donor polymer and an acceptor polymer are desirable in terms of their versatility in molecular design to tune light absorption and energy levels and have the advantage of better mechanical properties, morphological stability and ambient processability.[4–6] Consequently, all-polymer OPVs are a promising technology for applications in flexible devices and building integrated photovoltaics (BIPV) with the advantage that they can be manufactured with large-area printing techniques like roll-to-roll (R2R) processing. However, high efficiency OPVs are typically realized employing wasteful and non-scalable spin-coating in inert atmosphere. Fabricating devices by roll-to-roll compatible methods such as blade coating or slot-die coating is critical to translate OPVs to mass production to ultimately realize their potential of being a low-cost technology.[7] Unfortunately, often one cannot simply transfer the processing from spin-coating to R2R compatible techniques because device performance deteriorates[8] as the active layer morphology is highly sensitive to changes in processing conditions.[9] Specifically, for all-polymer

solar cells the polymeric acceptor typically has less tendency to form more intermixed and small domains with the polymer donor due to the strong tendency of the polymers to crystallize.[10] This results in poor morphological control and undesirable phase separation sizes much larger than the exciton diffusion length of 10–20 nm[11], leading to inefficient exciton splitting and poor performance. A few examples of high performance blade coated all-polymer solar cells have been demonstrated[12], but the gap in performance between spin-coated and blade-coated device performance remains. Thus, morphological control presents a key challenge in all-polymer solar cells, in particular developing processing to achieve adequately small nanophase seperation.[13,14]

In recent years, various strategies, including molecular design, solvent and thermal annealing, and solvent additives, have been employed to control morphology in spin-coated OPVs.[15–17] However, for all-polymer solar cells employing R2R-compatible fabrication techniques, precise control of morphology is rarely explored due to our relatively poor understanding of how processing impacts morphology[14], which limits R2R all-polymer solar cell application. One promising strategy to establish morphological control in blade and slot-die coated all-polymer OPVs is reducing the tendency of polymer to crystallize, potentially suppressing unfavorable phase separation.[18] This is particularly relevant to all-polymer OPVs featuring highly crystalline polymers and highlights the need to consider the polymers propensity to aggregate and crystallize during the film formation.[10] Specifically, we have shown recently that polymer blends with intrinsic low crystallinity feature highly stable morphology and reduced phase separated domain size, allowing for high-performance R2R printable solar cells.[18] Further, we demonstrated that incorporating 2,6-diisopropylphenyl as a fraction of the side-chains on a highly crystalline naphthalene diimide (NDI) based acceptor polymer effectively suppresses acceptor polymer crystallization resulting in reduced phase separation and improved all-polymer OPV performance.[19] Despite these approaches

showing great promise, high performance devices often use highly crystalline polymers and molecular design approaches to fine-tune crystallinity can be time intensive and expensive and may not result in the desired morphology control.

Herein, we demonstrate a simple yet effective solvent additive approach to control polymer crystallinity in a representative all-polymer OPV model system, PTB7-Th/P(NDI2OD-2T). Particularly P(NDI2OD-2T) is used in various spin-coated record performance all-polymer OPV systems,[20,21] but is prone to form large domains in polymer:P(NDI2OD-2T) blends due to the rigid and planar structures of NDI units and its strong tendency to aggregate.[22] For PTB7-Th/P(NDI2OD-2T), it has been reported that the high crystallinity of P(NDI2OD-2T) results in large domains (>300 nm) and poor performance in R2R-printed devices.[18] Therefore, moderating the polymer crystallization, molecular ordering and scale of phase separation is critical in P(NDI2OD-2T)-based all-polymer solar cells. However, established solvent additive such as 1,8-diiodooctane (DIO) and 1,8-octanedithiol (ODT) typically tend to induce polymer crystallinity, by extending drying times and possibly due to increased preferential solubility of the alkyl side chains of the polymers.[16] DIO has been shown to increase polymer crystallinity in PTB7-Th/P(NDI2OD-2T) resulting in highly ordered polymer organizations with face-on orientation.[23] Use of diphenyl ester (DPE) additive resulted in an increased domain size and reduced performance in blade-coated PBDBT-TS1/PPDIODT all-polymer solar cells.[14] Overall, there are very limited examples of effective solution additives for all-polymer solar cell systems[24], particularly for processing via blade-coating. Consequently, it is important to identify new solvent additive candidates that can better control polymer crystallization during solution printing to ultimately enable high performance printed all-polymer solar cells.

The majority of successful solvent additives typically have low volatility and selective solubility for either donor or acceptor.[16] Here, we explore the use of two phthalate additive candidates, diethyl phthalate (DEP) and dioctyl phthalate (DOP), to control crystallization and suppress unfavorable phase separation in a blade-coated all-polymer OPV model system (see Figure 1), PTB7-Th/P(NDI2OD-2T). Phthalates are commonly used as functional additives to improve flexibility, plasticity, and processability of polymer products by weakening intermolecular interactions and by lowering the overall crystallinity.[25] Further, phthalates typically feature relatively low volatility (bp > 300 °C) and large structural diversity. This structural diversity is of particular interest, as it can potentially be leveraged to fine tune polymer-additive interactions by systematically changing the molecular structure of the additive.[24]

In this paper, we explore the effects of the DEP and DOP additives on polymer crystallization and how they induce morphological changes in blade-coated neat and blend films of PTB7-Th and P(NDIOD-T2) using grazing incidence wide angle X-ray scattering (GIWAXS). We then used these additives to fabricate photovoltaic devices and showed that the additives indeed led to reduced blend crystallinity and higher PCE that are on-par with the best spin coated devices for the most effective additive. Morphological studies indirectly support that the phthalate additives enable a finer phase separation in all-polymer blends. Realtime X-ray scattering during blade-coating suggests that the DOP additive may act as a compatibilizer and suppresses unfavorable solid-liquid (S-L) phase separation.

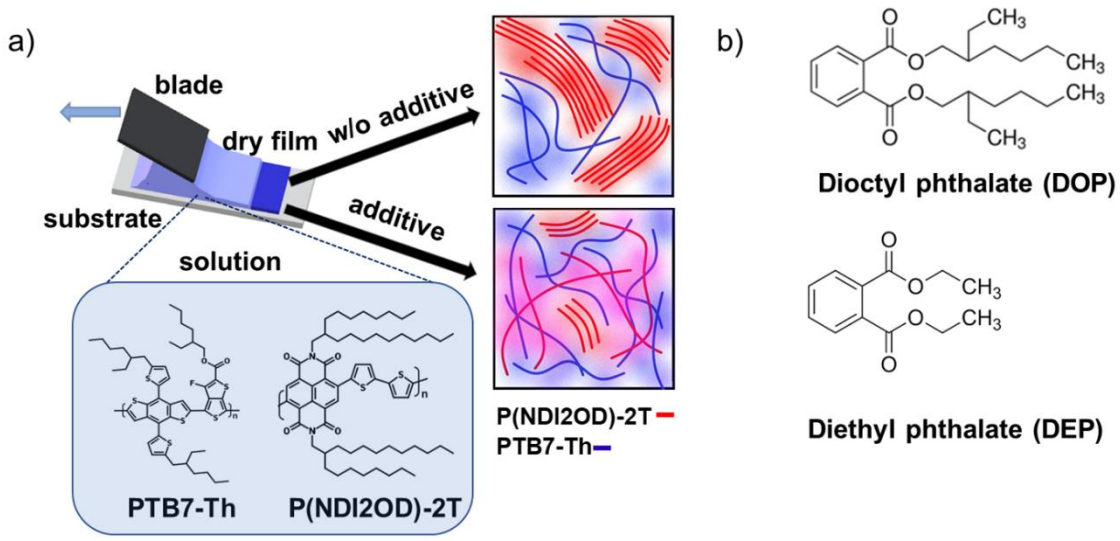

Figure 1: a) Schematic of blade-coated active layer morphology with and without additive b) Additive chemical structures.

2. Results and Discussion

2.1 All-Polymer Solar Cell Device Performance

We fabricated blade-coated, all-polymer solar cell devices using an inverted configuration of indium tin oxide (ITO)/ZnO (20 nm)/PTB7-Th:PNDI2OD-2T/MoO_3 (7.5 nm)/Ag (100 nm) to investigate the effect of the additive on device performance. The same optimized fabrication condition was used for all devices, specifically, D/A ratio (1:1 by weight), total solution polymer concentration (10 mg mL^{-1}) in chlorobenzene (CB) solvent, shearing speed (60 mm s^{-1}), processing temperature (60 °C), and film thickness (100 to 110 nm) of the active layer to reflect only the effect of the additive. Figure 2a shows the current density versus voltage (*J*–*V*) curves of the optimized device without additive and the best performing devices for each optimized amount of the respective additive under AM 1.5G illumination (100 mW cm^{-2}). The key photovoltaic metrics such as open-circuit voltage (V_{oc}), short-circuit current density (J_{sc}), fill factor (FF), and

power conversion efficiency (PCE) are summarized in Table 1 and are the statistical average of ten devices fabricated under the same conditions. The control devices fabricated by blade-coating without additive featured a low PCE of 2.09 % (V_{oc} = 0.766 V, J_{sc} = 5.16 mA cm^{-2}, and FF = 0.53), which is significantly lower than with best reported performances of spin-coated devices for this material system, with most reports ranging from 3.7% to 4.6%[20,26] and the record performance of 5.7%[27]. Notably, V_{oc} and FF of the blade-coated devices are comparable to reported values for spin coated OPVs. However, J_{sc} is significantly lower, suggesting a less optimal morphology and large domain size of the blade-coated devices.

Both additives improved the performance of the blade-coated devices. Additive concentrations of 0% v/v to 0.5% v/v have been explored. For the case of DEP additive 0.25% v/v exhibited marginally improved performance compared to 0.2% v/v but for easier comparison of device and morphological data between DEP and DOP additive we will limit the discussion to the 0.2% v/v case. Solar cells processed with the additives featured a relatively consistent V_{oc} almost independent of the additive treatment, varying from 0.77 to 0.79 V (Figure S1a). J_{sc} and PCE metrics were more relevant due to the pronounced changes depending on the additive being used. Remarkably, adding 0.20 v/v % of DEP additive resulted in an over two-fold increase of J_{sc} (11.2 mA cm^{-2}) and PCE (4.5 %). The increase of J_{sc} tracks well with the increase in PCE (Figure 2d). Interestingly, further increasing the amount of additive to 0.50% v/v resulted in a significant decrease in device performance, particularly for the DOP additive. Based on the device data, we expect that the significant increase in J_{sc} is due to a reduced phase separation size of donor and acceptor as a result from reduced aggregation of the individual polymers by the additives. The poor performance of devices cast with 0.5% v/v additive, is attributed to an overly disordered blend morphology as discussed below. To our knowledge this is the best performance for this

material system fabricated by blade-coating under ambient conditions, and is comparable to most of the best reported spin-coated devices.[20,26,27]

Table 1: Summary of key photovoltaic metrics of the blade coated all-polymer solar cells without additive and with 0.20% v/v DOP, 0.20% v/v DEP added to the casting solution under standard AM 1.5G 100 mW cm^{-2}.

Active layer	additive	*Voc*(V)	*Jsc*(mA/cm^2)	FF	PCE(%)[a]
PTB7-Th: P(NDI2OD-T2)	no	0.766 ± 0.01	5.16 ± 0.34	0.53 ± 0.01	2.09 ± 0.12
	DOP	0.791 ± 0.01	10.2 ± 0.29	0.51 ± 0.01	4.12 ± 0.10
	DEP	0.787 ± 0.01	11.2 ± 0.19	0.51 ± 0.01	4.50 ± 0.09

a) all parameters are the statistical average of ten devices under same conditions.

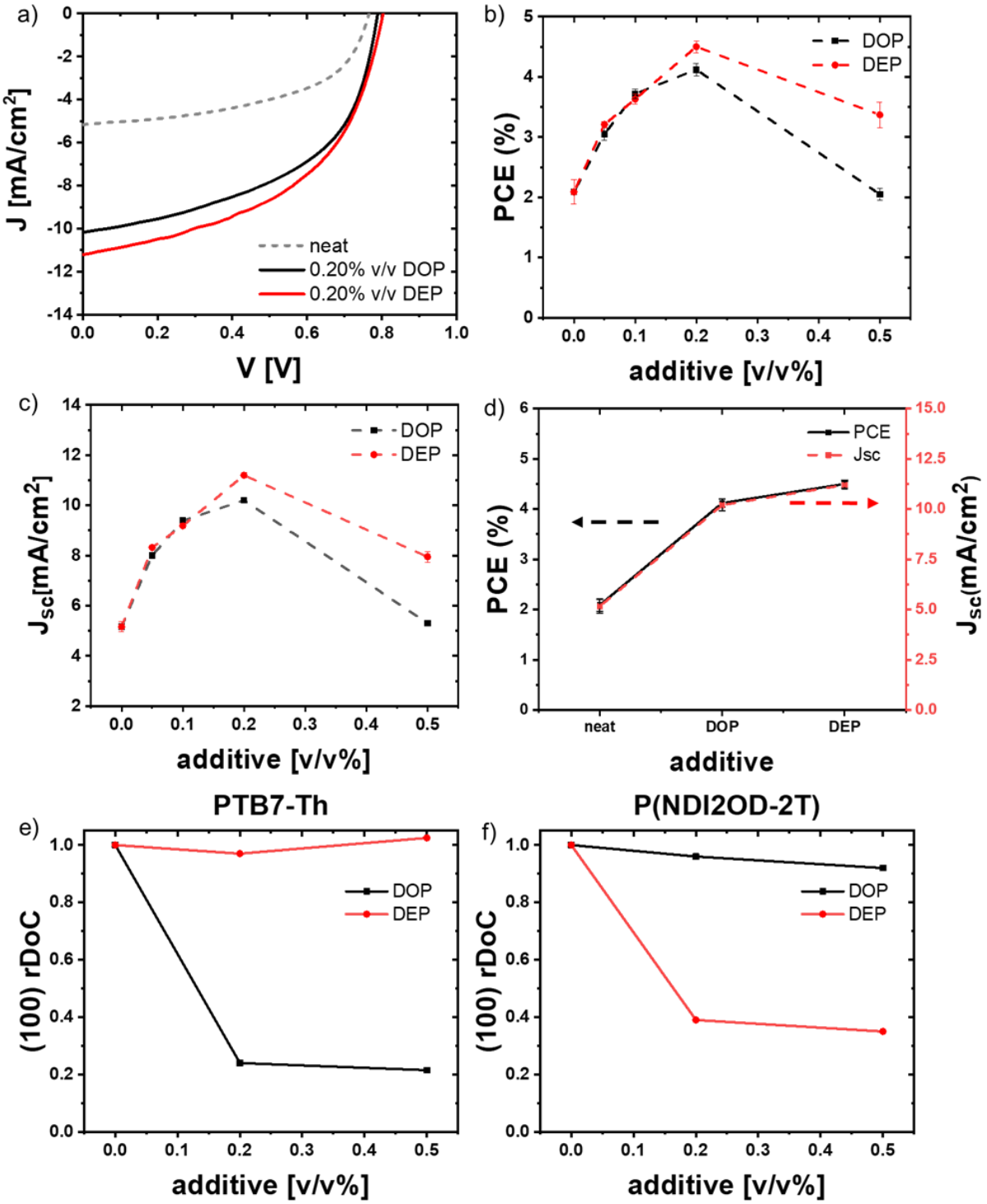

Figure 2: a) J-V characteristics of PTB7-Th/P(NDI2OD-2T) of optimized blends w/o (neat) and with DOP or DEP additive, b) PCE and c) J_{sc} as function of additive concentration for DOP and DEP additive. d) PCE and J_{sc} as function of additive (additive concentration of 0.2% v/v). RDoC of e) PTB7-Th and f) PNDI(2OD-2T) (100) lamellar peaks with 0% v/v, 0.2% v/v, and 0.5% v/v DOP and DEP.

2.2 Structural order and crystallinity of pristine donor and acceptor polymers

We performed GIWAXS of neat PTB7-Th (Figure 3a) and P(NDI2OD-2T) (Figure 3b) films with and without the additives to test our hypothesis. Specifically, we investigated how DOP and DEP additives affect the degree of crystallinity and packing in the polymer films. To accurately compare the scattering intensity of the pristine films in the GIWAXS patterns, we configured these images to have the same brightness and contrast and normalized the scattering intensity for sample size, film thickness, and incident X-ray beam intensity. GIWAXS measurements were performed parallel and perpendicular to the shearing direction, to confirm isotropic in-plane orientation of crystallites and to justify the applicability of the geometrical correction. All GIWAXS data shown is from measurements performed with the incident beam perpendicular to the shearing direction. Figure 3a shows the 2D-GIWAXS patterns of PTB7-Th cast from chlorobenzene solutions w/o (neat) or with 0.20%v/v DOP or 0.20%v/v DEP, which are close to the optimal values for device performance. In the neat film, PTB7-Th is weakly ordered and features predominantly face-on packing ($q(100) \approx 0.28$ Å^{-1} and $q(010) \approx 1.62$ Å^{-1}). Here we use (100), (010) and (001) to denote lamella, pi-stacking, and chain directions and planes, respectively. Upon addition of 0.20% v/v DOP additive, the intensity of both (100) and (010) peaks is significantly reduced, suggesting reduced crystallinity of PTB7-Th by DOP, while the predominantly face-on orientation is maintained. In contrast, the DEP additive did not have any significant effect on the crystallinity or orientation of PTB7-Th.

To quantify and further corroborate the qualitative effects of the additives on polymer crystallinity and orientation discussed above, we performed pole-figure and relative degree of crystallinity (rDoC) analysis of the polymer scattering patterns. The rDoC was calculated by

integrating the area of the geometrically corrected pole figures following procedures discussed in previous works.[28–31] Specifically, the scattering intensity of the (100) lamellar stacking peak and the (010) π–π stacking peak were background subtracted, integrated, normalized for irradiated sample volume and multiplied by the geometrical correction factor sin(χ) yielding pole-figures of the respective polymers.[31] The polar angle χ describes the relative orientation of crystallites with respect to the substrate normal, with the χ = 0˚ and 90˚ representing in-plane and out-of-plane respectively and thus for the (100) corresponding to edge-on and face-on orientation of crystallites. The scattering intensity of the (100) and (010) peaks were integrated over χ = [–85˚, 85˚] and the total integrated areas are compared between samples of PTB7-Th or P(NDI2OD-2T) with and without additive yielding their relative degree of crystallinity. Therefore, rDoC analysis captures the intensity of all crystallite orientations (χ = [–85˚, 85˚]) and not just the in-plane (100) peak intensity. Notably, 0.20%v/v DOP reduce the crystallinity of PTB7-Th by 77% ($rDoC_{(100)}$ = 0.23) (Figure 2e). Interestingly, further addition of DOP (0.5%v/v) does not significantly further reduce the crystallinity of PTB7-Th ($rDoC_{(100)}$ = 0.21). However, the overall orientation becomes more isotropic with an increasing fraction of edge-on orientation (Figure S2a). In contrast, adding 0.20%v/v and 0.50% v/v of DEP did not significantly affect orientation or rDoC of PTB7-Th (Figure S2b and 2e).

Figure 3b shows the 2D-GIWAXS patterns of PNDI2OD-2T cast from CB solutions w/o (neat), 0.20%v/v DOP or 0.20%v/v DEP additive added to the casting solution. In the neat film, P(NDI2OD-2T) is highly ordered and features predominantly face-on texture (q(100) ≈ 0.26 $Å^{-1}$, q(200) ≈ 0.52 $Å^{-1}$, q(010) ≈ 1.60 $Å^{-1}$ and q(001) ≈ 0.46 $Å^{-1}$), consistent with previous works.[32] Upon addition of the DOP or DEP additive, the in-plane intensity of the (100) peak and out-of-plane intensity of the (010) are significantly reduced. Notably, some ordering along the

P(NDI2OD-2T) backbone is maintained as evidenced by the (001) scattering observed in these samples. Interestingly, (100) and (010) pole figure (Figure S2) and rDoC analysis of P(NDI2OD-2T) samples reveal that the addition of 0.2 and 0.5%v/v DOP changes the orientation of P(NDI2OD-2T) from predominately face-on for 0.2%v/v DOP to more edge-on for 0.5% v/v DOP (Figure S3a), while the overall crystallinity is only slightly reduced ($rDoC_{(100)}$ = 0.92 for 0.5% v/v DOP) (Figure 2f). In contrast, the addition of 0.2 and 0.5% v/v DEP reduces the $rDoC_{(100)}$ of P(NDI2OD-2T) to 39% and 35% (Figure 2f), respectively, while maintaining the overall face-on orientation (Figure S3b).

Overall, the DOP and DEP additive have different effects on polymer crystallite orientation and crystallinity in PTB7-Th and P(NDI2OD-2T) films suggesting different interactions between the additives and the polymers. We speculate that these differences stem from differences in the additive-polymer interactions related to the subtle differences in DEP and DOP additive molecular structures.

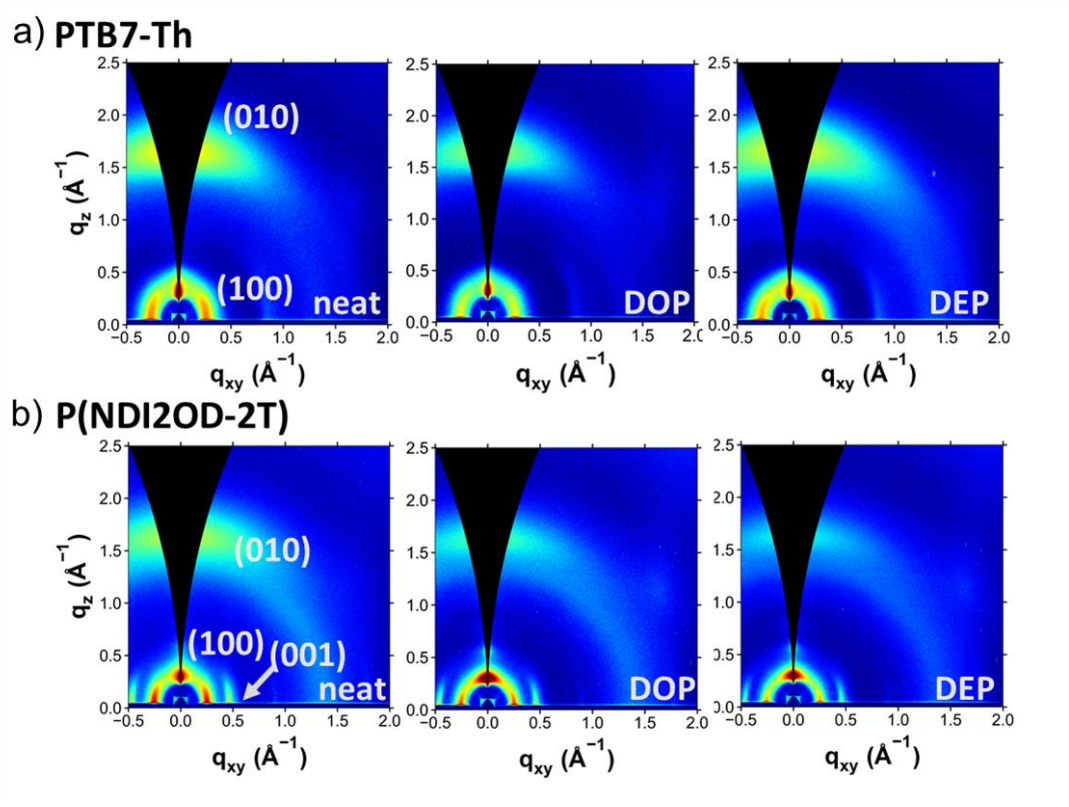

Figure 3: a) 2D-GIWAXS patterns for PTB7-Th and b) P(NDI2OD-T2) films sheared from CB solutions w/o additive, 0.2%v/v DOP, 0.20%v/v DEP.

2.3 Structural order and crystallinity of PTB7-Th/P(NDI2OD-2T) blends

We then performed GIWAXS of PTB7-Th/P(NDI2OD-2T) blend films (Figure 4a) with and without the respective additives to understand the effect of the additives on blend morphology. As for the neat films, we configured these images (measured perpendicular to shearing direction) to have the same brightness and contrast and normalized the scattering intensity for sample size, film thickness, and incident X-ray beam intensity to accurately compare the scattering intensity of all the pristine films in the GIWAXS patterns. Overall, we observe preferential face-on orientation of all the blends, with and without additives (see Figure 4a). The similar *q* position of (100) and (010) peaks of donor ($q(100) \approx 0.28$ Å^{-1}, $q(010) \approx 1.62$ Å^{-1}) and the acceptor ($q(100) \approx 0.26$ Å^{-1}, $q(010) \approx 1.60$ Å^{-1}) polymers made it difficult to evaluate

the crystallinity and packing of the individual polymers (see Figure S5). However, we observe scattering in-plane at q = 0.46 $Å^{-1}$, which is unambiguously due to the (001) peak of P(NDI2OD-2T), indicating that some P(NDI2OD-2T) is ordered in the blend. Qualitatively, both additives disorder the polymers within the blend compared to neat films as evidenced by the reduced scattering intensity of the (100), (010), and (001) peaks.

rDoC analysis reveals that both 0.20% v/v DEP or DOP additive reduce blend crystallinity of the polymers by about 50% (rDoC ≈ 0.5) (see Figure 4b). Here by blend crystallinity we mean the combined P(NDIOD-2T) and PTB7-Th crystallinities, since we cannot distinguish individual components. Increasing the amount of DEP and DOP additive to 0.50% v/v slightly decreases blend crystallinity, but does not further improve device performance. We observe a decrease in device performance (see Figure 4c) for 0.5% v/v DOP or DEP which may be attributed to an overly disordered blend morphology, as evidenced both by further slightly decreased rDoC and a less face-on orientation of the polymers (see Figure S4a and S4b). Generally, face-on orientation is considered favorable for OPVs, facilitating efficient hole and electron transport between the electrodes, which is beneficial to device performance.[23,33] Notably, the loss of predominantly face-on orientation is more pronounced for the DOP additive in line with the more pronounced decrease in performance for 0.5% v/v DOP (Figure 4c).

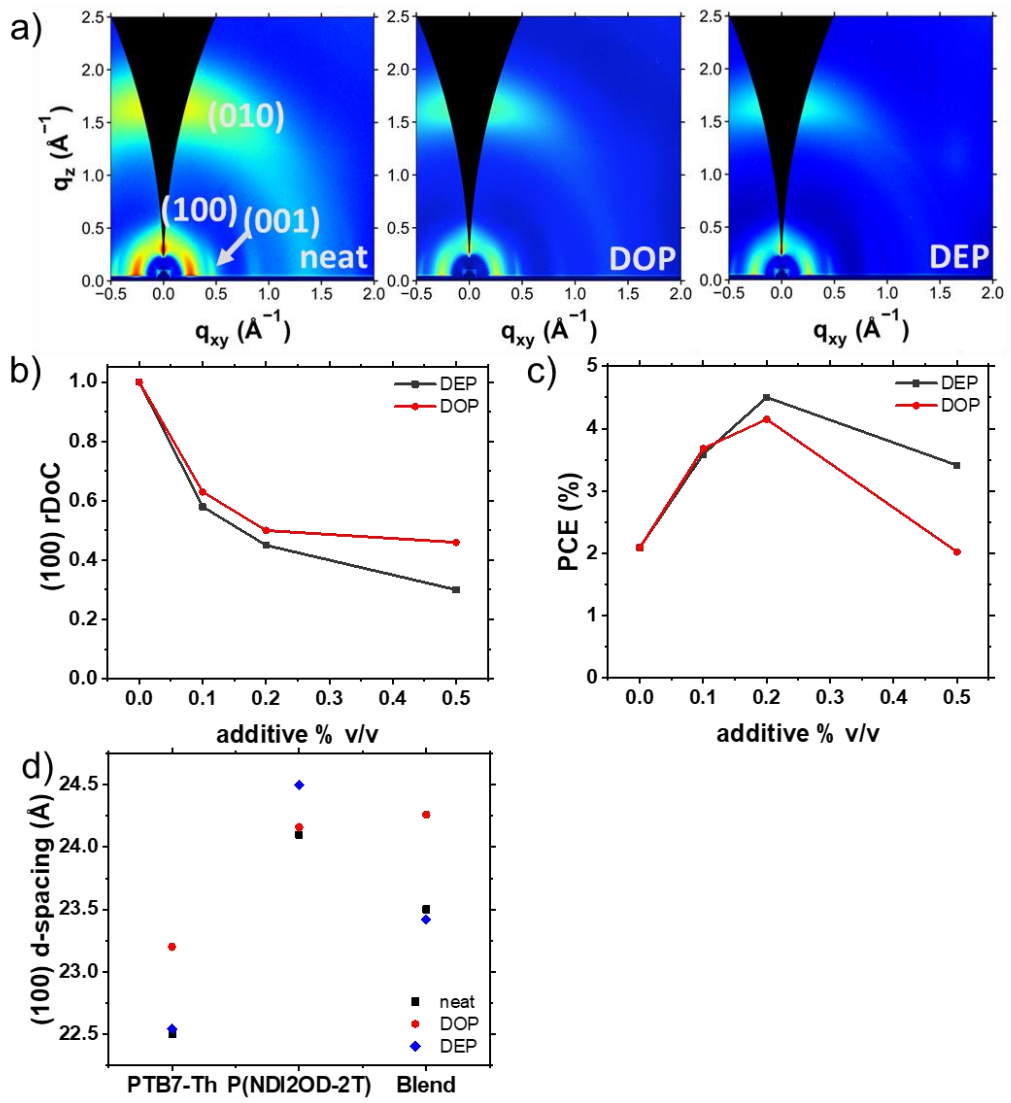

Figure 4: a) 2D-GIWAXS patterns for PTB7-Th/P(NDI2OD-T2) blend films sheared from CB solutions w/o additive, 0.2%v/v DOP, and 0.2%v/v DEP. b) rDoC for the lamellar (100) peak of blend films with varying amounts of DEP and DOP additive c) PCE of blend films with varying amounts of DEP and DOP additive. d) (100) d-spacing of PTB7-Th, P(NDI2OD-2T) and blend w/o additive (neat), DOP and DEP.

As discussed above, DEP reduces the crystallinity of neat P(NDI2OD-2T) films but does not significantly affect the neat PTB7-Th crystallinity. The DOP additive strongly decreases PTB7-Th crystallinity while the crystallinity of P(NDI2OD-2T) was less affected. However, DOP makes the orientation of P(NDI2OD-2T) less face-on and more isotropic. Further, as mentioned above, the q-positions of donor and acceptor nearly overlap. Therefore the (100) d-

spacing in the blend is a combination of both donor and acceptor lamella peaks. Comparing the (100) peak positions of PTB7-Th and P(NDI2OD-2T) in neat and blend films reveals that DOP predominantly disordered PTB7-Th in the blend (Figure S6), as evidenced by the (100) d-spacing of the blend with DOP additive (24.5 Å) closely resembling the d-spacing of neat P(NDI2OD-2T) (24.3 Å) (Figure 4d). Interestingly, the (100) d-spacing of the blend with DEP additive (23.4 Å) is nearly identical to the d-spacing of the blend without additive (23.5 Å) suggesting that *both* the donor and acceptor polymers have similar crystallinity in the blend yielding a more balanced crystallinity between donor and acceptor. By balanced crystallinity we refer to the scenario where both donor and acceptor have comparable degrees of crystallinity in the blend in contrast to a scenario where one material is highly crystalline, and the other material is amorphous. Balancing crystallinity has been shown to be an effective strategy to achieve small scale phase separation and balanced charge carrier mobilities, enabling high device performance. Specifically, balanced carrier mobilities have been shown to contribute to a high FF and device performance.[19,34,35] The slightly superior performance of the DEP additive as compared to DOP is attributed to the more balanced crystallinity and slightly higher FF for the blend cast with the DEP additive. We further acquired atomic force microscopy (AFM) images of blend films to investigate the qualitative effects of the additive on the blend active layer surface morphology. The topography image of the PTB7-Th:P(NDI2OD-2T) blend without additive (Figure S7a) show large and elongated structures which may be related to fibrillar polymer structure, often observed for P(NDI2OD-2T). The extend of these surface structures appears to be reduced for the DOP additive (Figure S7b) and the blend cast with DEP additive (Figure S7c) features a significantly different surface morphology with smaller features suggesting the absence of large P(NDI2OD-2T) fibrillar polymer structures and improved phase separation size.

Findings from morphology characterization further indirectly support our hypothesis that DOP and DEP additive reduce phase separation size between donor and acceptor polymers based on the strong correlation of increase in performance with increase in J_{sc}. To further corroborate the effects of the additives on the donor acceptor phase separation size in blends, we performed resonant soft X-ray scattering (RSoXS) measurements. However, it was not possible to resolve any clear features for blends with and without additives. This is likely due to the limited contrast between donor and acceptor for all-polymer blends and to the convolution of orientation and domain contrast.

2.3 Influence of Additive on Real-Time Polymer Aggregation during Solution Printing

To gain an in-depth understanding and provide mechanistic insight for the morphology evolution during solution printing, we used real-time in-situ X-ray diffraction during blade-coating[36] (see Figure 5a) to track the crystallization process of PTB7-Th and P(NDI2OD-2T) polymers w/o and with the additives. We perform peak fitting of the (100) polymer peak at various times of wet film drying to extract the (100) peak area. The increase in the (100) peak area is proportional to the amount of crystalline polymer that is formed. Neat PTB7-Th films were found to be too weakly scattering for the in-situ experiments, particularly with DOP additive added. Hence, we limit this discussion to the crystallization kinetics of P(NDI2OD-2T) and PTB7-Th/P(NDI2OD-2T) blends. Figures 5b shows representative GIWAXS line-cut profiles at various times during film drying for thin-films printed from P(NDI2OD-2T) solutions. Figure 5c shows the evolution of the (100) P(NDI2OD-2T) polymer peak during film drying. To aid the discussion of the crystallization kinetics, we propose a four-stage model to describe the film drying: (I) dissolution stage, (II) aggregation stage, (III) nucleation and rapid growth stage, and (IV) final

film stage. Further, we define the duration of the respective stages I-IV as t_stage. In the beginning of the wet film drying (stage I), P(NDI2OD-2T) remained well-dissolved and no diffraction was observed. As the solvent continues to evaporate, the concentration of the polymer increases, and P(NDI2OD-2T) reaches its solubility limit in chlorobenzene. This typically results in polymer aggregation and nucleation as evidenced the appearance of the (100) diffraction peak (stage II and III).[10] Stage IV represents the final film stage which is reached once nucleation and growth process stop and the solvent is fully evaporated.

Figure 5c shows the peak fitting of the (100) polymer peak of P(NDI2OD-2T) cast from a 5 mg mL^{-1} CB solution. This concentration was chosen as it is the effective concentration of P(NDI2OD-2T) in PTB7-Th/P(NDI2OD-2T) blend solutions (10 mg/mL, D/A ratio = 1:1). In stage I the overall scattering is dominated by the scattering from CB solvent and exhibits a broad isotropic diffraction feature centered at $q \approx 1.4$ $Å^{-1}$ with no polymer scattering observed. After 13s of wet-film drying, we observe aggregation of P(NDI2OD-2T) in stage II as evidenced by the appearance of a scattering feature at $q \approx 0.248$ $Å^{-1}$ with a larger d-spacing ($d_{aggregate} \approx 25.3$ Å) than in the fully dried film ($d_{xtal} \approx 24.3$ Å). These aggregates are ordered but are still swollen with solvent, as evidenced by the increased d-spacing.[37] Strong self-aggregation and crystallization of P(NDI2OD-2T) often results in large crystalline domains in blends with a much weaker aggregating donor like PTB7-Th[38] and PPDT2FBT[39]. With ongoing solvent evaporation, we observe a gradual increase of the scattering intensity of these P(NDI2OD-2T) aggregates. At 21s, we observe the onset of P(NDI2OD-2T) crystallite nucleation and growth (stage III), which becomes evident from the distinct change in observed d-spacing from ≈ 25.3 Å to ≈ 24.3 Å (final film $d_{xtal} \approx 24.3$ Å) and change in the slope. During this time, reflections characteristic of the formation of face-on crystallites, including the (010) π–π stacking peak in the out-of-plane direction and the (100)

lamellar stacking peak in the in-plane direction, appeared and rapidly increased in intensity. At 27.5 seconds nucleation and growth concludes ($t_{III} \approx 6$ s) and stage IV is reached. Figure 5d and Figure 5e show the peak fitting results of the (100) polymer peak of P(NDI2OD-2T) cast from CB solutions with 0.20% v/v and 0.50% v/v DEP additive, respectively. For 0.2% v/v DEP, we observe a slight reduction of the extend of aggregation in stage II, as evidenced by delayed onset and overall reduced scattering intensity of stage II. These changes become more apparent for 0.50% v/v DEP. The polymer pre-aggregation in stage II is suppressed, and nucleation and growth during stage III becomes more gradual, as evidenced by the reduced slope of the (100) peak area evolution (Figure 5e) and the lack of a change in d-spacing. The drastic change in curve shape (between no additive and 0.5% v/v DEP) further supports different crystallization behaviors due to the additive. The S-like curve shape for the 0.5% v/v DEP case represents continuous nucleation and growth[40], distinct from the rapid nucleation and growth stage without the additive. Moderating the strong self-aggregation of P(NDI2OD-2T) is critical for efficient OPVs, as strong self-aggregation was found to reduce the intermixing of acceptor and donor polymers, resulting in an excessively large phase separation between donor and acceptor beyond the exciton diffusion length.[22]

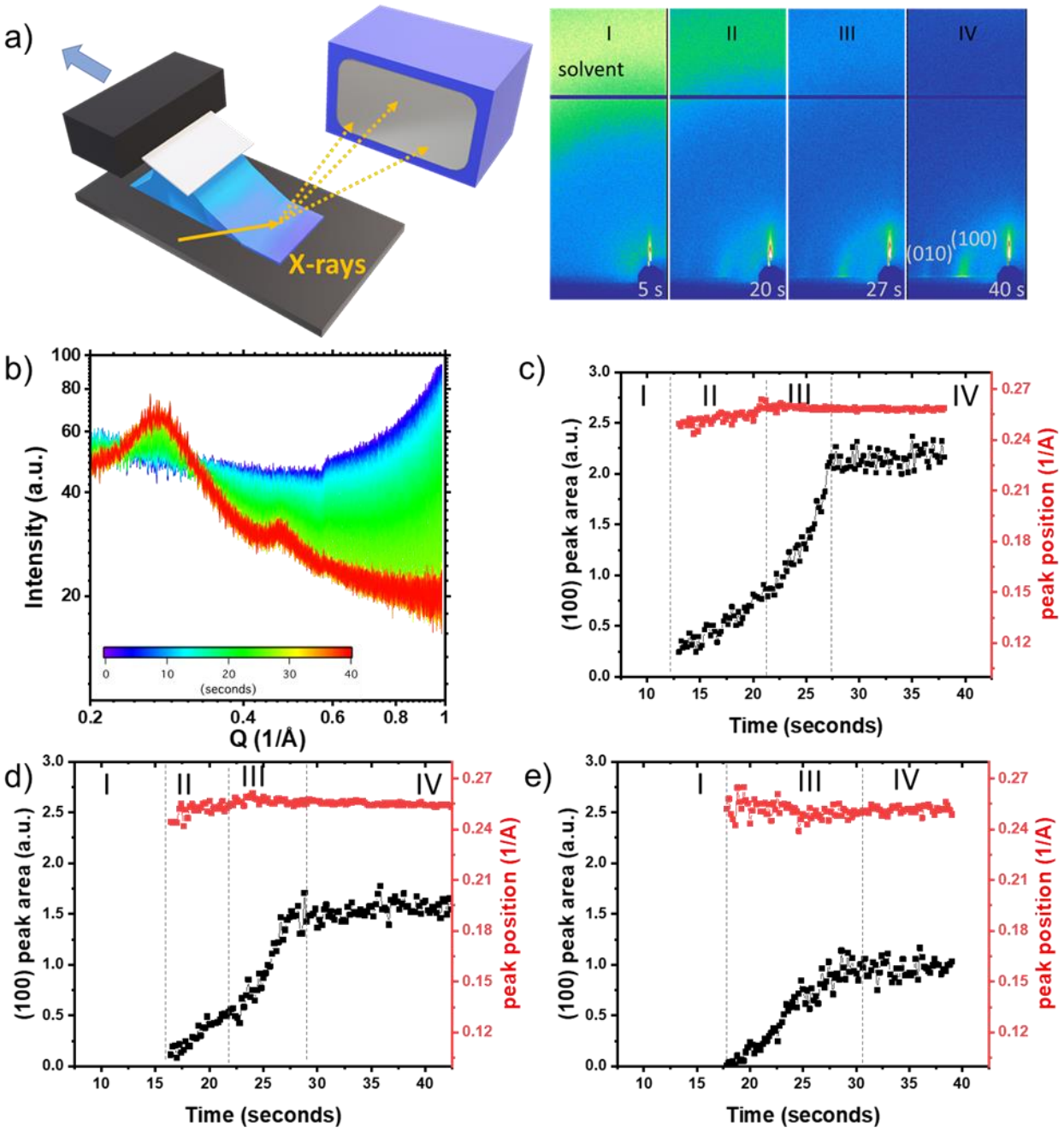

Figure 5: a) Schematic of the real-time in-situ X-ray diffraction during blade coating setup with representative 2D GIWAXS images at different times of the drying process. b) Representative in-situ GIWAXS in-plane line-cut profiles of the P(NDI2OD-2T) wet-film drying process. (100) peak fitting results of in-situ GIWAXS of P(NDI2OD-2T) c) without additive, d) with 0.2% v/v DEP, and e) with 0.5% v/v DEP additive cast from 5 mg mL^{-1} solutions. (I) dissolution stage, (II) aggregation stage, (III) nucleation and growth stage, and (IV) final film stage. The approximate boundaries between the respective stages are shown by white dashed lines as a guide. The extracted parameters (peak location and peak area) of the (100) peak are calculated by Gaussian fitting of the 1D scattering profiles from in-situ GIWAXS.

In the following we studied the effects of the DOP additive on the all-polymer blend. The similar q position of (100) and (010) peaks of donor ($q(100) \approx 0.28$ Å^{-1}, $q(010) \approx 1.62$ Å^{-1}) and the acceptor ($q(100) \approx 0.26$ Å^{-1}, $q(010) \approx 1.60$ Å^{-1}) polymers made it difficult to evaluate the crystallinity and packing of the individual polymers printed from blend solutions for our in situ experiments. Hence, peak fitting of the composite (100) peak of both polymers is evaluating the overall crystallization behavior of both donor and acceptor. We observed rapid polymer crystallization (stage III) in the blend without additive (see Figure 6) with a crystallization onset at about 12 s after the deposition of the wet film and completion of crystallization after a further 6.5 s ($t\_{III} \approx 6.5$ s). Notably, the DOP additive yields a two-fold increase in the time to complete nucleation and growth during stage III ($t_{stage\ III} \approx 13.5$ s) and overall reduced peak area or crystallinity in line with what was observed in ex-situ morphology characterization discussed above. To better quantify the effects of the DOP additive on the crystallization kinetics, we calculated the rate of crystallization by extracting the linear slope of the (100) peak area vs time plots during nucleation and growth in stage III (Figure S8). We use the (100) peak area as a proxy for the amount of crystalline polymer that is formed. The addition of DOP results in a significant reduction on the crystallization rate (0.087 arb. units/s) compared to the case without the DOP additive (0.19 arb. units /s). Note the GIWAXS intensities are in arbitrary units (au) and these are the same for both additives. We further performed Fourier-transform infrared spectroscopy (FT-IR) to determine residual amounts of additive after solution casting (Figure S9). We don't observe any significant differences in the spectra of blend films cast with DOP or DEP and w/o additive suggesting that most of the additives evaporate during solution casting and during thermal evaporation of the top-electrodes at low pressures (5×10^{-6} Torr). Given the limited sensitivity of the FT-IR technique and previous reports showing residual trace amounts of the lower boiling

point additive 1,8-diiodooctane (DIO) in active layers cast with DIO additive[41,42], however, we acknowledge that small amounts of DEP and DOP additives may still remain in the active layers. Given that most of the DOP and DEP additives can evaporate during solution casting we primarily attribute the improved morphology to the additives effects on the morphology evolution during printing but residual additive may play a role in stabilizing and compatibilizing donor and acceptor phases in the final film morphology. Consequently, evaporation of residual additive during long-term operation may negatively affect the morphological stability of the devices.

During solvent evaporation, liquid–liquid (L–L) and/or solid–liquid (S–L) demixing are the primary competing processes that drive phase separation and strongly influence the final blend morphology.[14,16] S–L demixing occurs when either donor or acceptor aggregates after reaching its solubility limit or supersaturation in the blend solution. Polymers with a strong tendency to crystallize like P(NDI2OD-2T) (as discussed above) tend to segregate easily in solution. Slow solvent evaporation, which is typically the case in blade-coating as compared to spin-coating, enables prolonged aggregation. This increases the extent of S–L demixing and can result in coarser

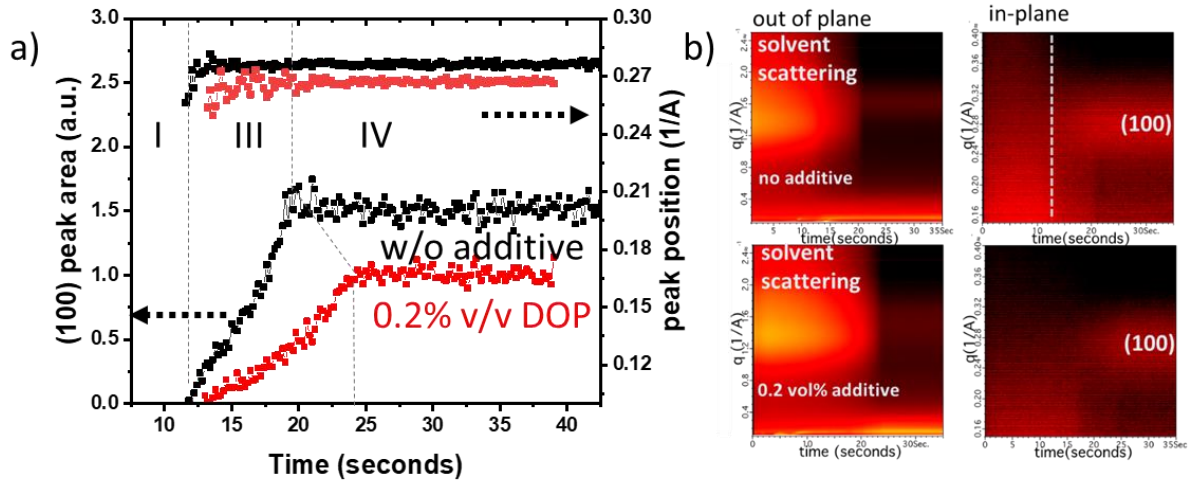

Figure 6: a) (100) peak area and position of blend in-situ GIWAXS. b) q vs. time plots of blend with and without additive showing solvent scattering (solvent drying). Dashed line is guide to the eye indicating the onset of crystallization. The extracted parameters (peak location and peak area) of the (100) peak are calculated by Gaussian fitting of the 1D scattering profiles from in-situ GIWAXS.

phase separation and low device performance. Additives acting as compatibilizers can reduce the repulsive forces between the donor and acceptor as well as polymer crystal growth rate, thereby reducing unfavorable L-L or S-L phase separation.[16] Another possible mechanism for additives is to act as nucleating agents. In the context of solvent additives, nucleation agents have been used to manipulate the initial nucleation density in some BHJ systems by reducing the nucleation barrier[16,43] and consequently increasing the nucleation rate and typically increase the rate of crystallization[44]. Based on our observation of a delayed and slower crystallization (reduced crystallization rate), we rule out the possible nucleation agent behavior of the DOP additive. It is suggested that DOP may act as compatibilizer between the two polymers, reducing the demixing of donor and acceptor polymer resulting in smaller phase separation, which is in line with our device and morphology data. Specifically, the compatibilization effect of DOP may mediate the repulsive force between PTB7-Th and P(NDI2OD-2T), enabling entanglement and mixing of the donor and acceptor polymers, reducing the polymers propensity to self-aggregate. Overall, it is suggested that the addition of 0.2% v/v DOP suppresses unfavorable phase separation by preventing polymer aggregation and S–L demixing in the BHJ solution, ultimately enabling a more favorable active layer morphology with finer phase separation and improved device performance.

These morphological changes agree well with our device characterization. As discussed above, the addition of 0.20 v/v % of additive (DOP or DEP) resulted in an over two-fold increase of J_{sc} and PCE. The significant increase of J_{sc} tracks well with the increase in PCE, in line with a reduced phase separation size of donor and acceptor in active layers printed from BHJ solutions with the phthalate additives.

3 Conclusions

In conclusion, we have demonstrated a new solvent additive approach employing two phthalate additive candidates, DEP and DOP, to control polymer crystallinity to suppress unfavorable phase separation in a representative PTB7-Th/P(NDI2OD-2T) all-polymer blend resulting in an over two-fold improvement of the blade-coated device performance from 2.09% to 4.50% fabricated in ambient conditions using DEP as solvent additive. The device performance compares well to record spin coated devices in the literature highlighting the effectiveness of the approach. Thus, the use of the DEP or DOP additive effectively mitigate the loss in performance that is often observed in translating from spin-coating to blade coating fabrication. Developing methods to control polymer crystallization and phase separation are critical to translating high performance all-polymer solar cells featuring highly crystalline polymers like the commonly used P(NDI2OD-2T) to scalable R2R compatible fabrication techniques like blade-coating. Phthalate additives feature a large structural diversity, which can potentially be leveraged to fine-tune polymer additive interactions by systematically changing the molecular structure of the additive. Consequently, this simple yet effective concept is promising for application in other all-polymer systems.

Experimental Section

PTB7-Th and P(NDI2OD-T2) were obtained from 1-Material, Inc. and were used as received. The M_n and $Đ_M$ of polymers were measured by high-temperature GPC with 1,2,4-trichlorobenzene as the eluent and polystyrenes as the calibration standards at 180 °C. The molecular weight was M_n = 57.5 kDa for PTB7-Th and M_n = 76.0 kDa P(NDI2OD-T2). All solvents and additives were purchased from Sigma Aldrich. All-polymer solar cells were fabricated in an inverted device architecture comprising glass/ITO/ZnO/active layer/MoO3/Ag. The active layer was deposited via solution shearing at a substrate temperature of 60 °C from CB solution with D/A

ratio of 1:1 (by weight) and total solution polymer concentration (10 mg mL^{-1}) in ambient air. The MoO_3 layer (7.5 nm) followed by an Ag layer (100 nm) were thermally deposited at a pressure of 5×10^{-6} Torr. Solar cell device metrics were acquired under AM 1.5G illumination with an intensity of 100 mW cm^{-2} under nitrogen atmosphere. GIWAXS images were collected at beamline 11-3 of the Stanford Synchrotron Radiation Lightsource (SSRL). The sample-to-detector distance was 315 mm, and the incidence angle was 0.14°; the X-ray wavelength was 0.9758 Å, corresponding to a beam energy of 12.7 keV. Samples for X-ray characterization were sheared on bare Si wafer using the same conditions as for device fabrication. In-situ GIWAXS images were collected at beamline 7-2 of the SSRL. AFM images were acquired in tapping mode using a Park NX-10 AFM. FT-IR absorption spectra were recorded using a Nicolet iS50 FT/IR Spectrometer in attenuated total reflectance (ATR) mode. The full experimental procedures are shown in the Supporting Information.

Supporting Information

- Materials, Solar Cell Fabrication, Device Performance Characterization, Morphology Characterization, Voc and FF as a function of additive concentration, PTB7-Th pole figures, P(NDI2OD-2T) pole figures, blend pole figures, in-plane and out of plane 1D GIWAXS linecuts, AFM images of blend w/o and with additive, linear fits of crystallization kinetics, and FT-IR spectra of pure additives and blend active layers with and w/o additive

Author Information

Corresponding author:

Michael F. Toney - michael.toney@colorado.edu

Acknowledgements

We acknowledge financial support from the Office of Naval Research (Program manager P. Armistead, award N00014-17-1-2214). Use of the Stanford Synchrotron Radiation Lightsource, SLAC National Accelerator Laboratory, is supported by the U.S. Department of Energy, Office of Science, Office of Basic Energy Sciences under contract no. DE-AC02-76SF00515. This research used resources of the Advanced Light Source, a U.S. DOE Office of Science User Facility under contract no. DE-AC02-05CH11231. Part of this work was performed at the Stanford Nano Shared Facilities (SNSF), supported by the National Science Foundation under award ECCS-1542152.

References:

(1) Zhang, M.; Zhu, L.; Zhou, G.; Hao, T.; Qiu, C.; Zhao, Z.; Hu, Q.; Larson, B. W.; Zhu, H.; Ma, Z.; et al. Single-Layered Organic Photovoltaics with Double Cascading Charge Transport Pathways: 18% Efficiencies. *Nat. Commun.* **2021**, *12* (1), 1–10. https://doi.org/10.1038/s41467-020-20580-8.

(2) Liu, T.; Yang, T.; Ma, R. Article 16 % Efficiency All-Polymer Organic Solar Cells Enabled by a Finely Tuned Morphology via the Design of Ternary Blend Cells Enabled by a Finely Tuned Morphology via the Design of Ternary Blend. *Joule* **2021**, 1–17. https://doi.org/10.1016/j.joule.2021.02.002.

(3) Fu, H.; Li, Y.; Yu, J.; Wu, Z.; Fan, Q.; Lin, F.; Woo, H. Y.; Gao, F.; Zhu, Z.; Jen, A. K. Y. High Efficiency (15.8%) All-Polymer Solar Cells Enabled by a Regioregular Narrow Bandgap Polymer Acceptor. *J. Am. Chem. Soc.* **2021**, *143* (7), 2665–2670. https://doi.org/10.1021/jacs.0c12527.

(4) Kim, T.; Kim, J.-H.; Kang, T. E.; Lee, C.; Kang, H.; Shin, M.; Wang, C.; Ma, B.; Jeong, U.; Kim, T.-S.; et al. Flexible, Highly Efficient All-Polymer Solar Cells. *Nat. Commun.* **2015**, *6*, 8547. https://doi.org/10.1038/ncomms9547.

(5) Xu, Y.; Yuan, J.; Zhou, S.; Seifrid, M.; Ying, L.; Li, B.; Huang, F.; Bazan, G. C.; Ma, W. Ambient Processable and Stable All-Polymer Organic Solar Cells. *Adv. Funct. Mater.* **2019**, *29* (8), 1806747. https://doi.org/10.1002/adfm.201806747.

(6) Facchetti, A. Polymer Donor–Polymer Acceptor (All-Polymer) Solar Cells. *Mater. Today* **2013**, *16* (4), 123–132. https://doi.org/10.1016/j.mattod.2013.04.005.

(7) Søndergaard, R.; Hösel, M.; Angmo, D.; Larsen-Olsen, T. T.; Krebs, F. C. Roll-to-Roll Fabrication of Polymer Solar Cells. *Mater. Today* **2012**, *15* (1–2), 36–49. https://doi.org/10.1016/S1369-7021(12)70019-6.

(8) Bundgaard, E.; Livi, F.; Hagemann, O.; Carlé, J. E.; Helgesen, M.; Heckler, I. M.; Zawacka, N. K.; Angmo, D.; Larsen-Olsen, T. T.; dos Reis Benatto, G. A.; et al. Matrix Organization and Merit Factor Evaluation as a Method to Address the Challenge of

Finding a Polymer Material for Roll Coated Polymer Solar Cells. *Adv. Energy Mater.* **2015**, *5* (10), 1402186. https://doi.org/10.1002/aenm.201402186.
(9) Ro, H. W.; Downing, J. M.; Engmann, S.; Herzing, A. A.; DeLongchamp, D. M.; Richter, L. J.; Mukherjee, S.; Ade, H.; Abdelsamie, M.; Jagadamma, L. K.; et al. Morphology Changes upon Scaling a High-Efficiency, Solution-Processed Solar Cell. *Energy Environ. Sci.* **2016**, *9* (9), 2835–2846. https://doi.org/10.1039/C6EE01623E.
(10) Gu, X.; Yan, H.; Kurosawa, T.; Schroeder, B. C.; Gu, K. L.; Zhou, Y.; To, J. W. F.; Oosterhout, S. D.; Savikhin, V.; Molina-Lopez, F.; et al. Comparison of the Morphology Development of Polymer-Fullerene and Polymer-Polymer Solar Cells during Solution-Shearing Blade Coating. *Adv. Energy Mater.* **2016**, *6* (22), 1601225. https://doi.org/10.1002/aenm.201601225.
(11) Heeger, A. J. 25th Anniversary Article: Bulk Heterojunction Solar Cells: Understanding the Mechanism of Operation. *Adv. Mater.* **2014**, *26* (1), 10–28. https://doi.org/10.1002/adma.201304373.
(12) Lin, B.; Zhang, L.; Zhao, H.; Xu, X.; Zhou, K.; Zhang, S.; Gou, L.; Fan, B.; Zhang, L.; Yan, H.; et al. Molecular Packing Control Enables Excellent Performance and Mechanical Property of Blade-Cast All-Polymer Solar Cells. *Nano Energy* **2019**, *59*, 277–284. https://doi.org/10.1016/j.nanoen.2019.02.046.
(13) Lee, C.; Li, Y.; Lee, W.; Lee, Y.; Choi, J.; Kim, T.; Wang, C.; Gomez, E. D.; Woo, H. Y.; Kim, B. J. Correlation between Phase-Separated Domain Sizes of Active Layer and Photovoltaic Performances in All-Polymer Solar Cells. *Macromolecules* **2016**, *49* (14), 5051–5058. https://doi.org/10.1021/acs.macromol.6b01069.
(14) Ye, L.; Xiong, Y.; Li, S.; Ghasemi, M.; Balar, N.; Turner, J.; Gadisa, A.; Hou, J.; O'Connor, B. T.; Ade, H. Precise Manipulation of Multilength Scale Morphology and Its Influence on Eco-Friendly Printed All-Polymer Solar Cells. *Adv. Funct. Mater.* **2017**, 1702016. https://doi.org/10.1002/adfm.201702016.
(15) Liao, H.-C.; Ho, C.-C.; Chang, C.-Y.; Jao, M.-H.; Darling, S. B.; Su, W.-F. Additives for Morphology Control in High-Efficiency Organic Solar Cells. *Mater. Today* **2013**, *16* (9), 326–336. https://doi.org/10.1016/J.MATTOD.2013.08.013.
(16) McDowell, C.; Abdelsamie, M.; Toney, M. F.; Bazan, G. C. Solvent Additives: Key Morphology-Directing Agents for Solution-Processed Organic Solar Cells. *Adv. Mater.* **2018**, *30* (33), 1707114. https://doi.org/10.1002/adma.201707114.
(17) Zhao, F.; Wang, C.; Zhan, X. Morphology Control in Organic Solar Cells. *Adv. Energy Mater.* **2018**, *8* (28), 1703147. https://doi.org/10.1002/aenm.201703147.
(18) Gu, X.; Zhou, Y.; Gu, K.; Kurosawa, T.; Guo, Y.; Li, Y.; Lin, H.; Schroeder, B. C.; Yan, H.; Molina-Lopez, F.; et al. Roll-to-Roll Printed Large-Area All-Polymer Solar Cells with 5% Efficiency Based on a Low Crystallinity Conjugated Polymer Blend. *Adv. Energy Mater.* **2017**, *7* (14), 1602742. https://doi.org/10.1002/aenm.201602742.
(19) Wu, Y.; Schneider, S.; Walter, C.; Chowdhury, A. H.; Bahrami, B.; Wu, H.-C.; Qiao, Q.; Toney, M. F.; Bao, Z. Fine-Tuning Semiconducting Polymer Self-Aggregation and Crystallinity Enables Optimal Morphology and High-Performance Printed All-Polymer Solar Cells. *J. Am. Chem. Soc.* **2020**, *142* (1), 392–406. https://doi.org/10.1021/jacs.9b10935.
(20) Wang, G.; Melkonyan, F. S.; Facchetti, A.; Marks, T. J. All-Polymer Solar Cells: Recent Progress, Challenges, and Prospects. *Angew. Chemie Int. Ed.* **2019**, *58* (13), 4129–4142. https://doi.org/10.1002/anie.201808976.

(21) Zhou, N.; Facchetti, A. Naphthalenediimide (NDI) Polymers for All-Polymer Photovoltaics. *Mater. Today* **2018**, *21* (4), 377–390. https://doi.org/10.1016/J.MATTOD.2018.02.003.
(22) Schubert, M.; Dolfen, D.; Frisch, J.; Roland, S.; Steyrleuthner, R.; Stiller, B.; Chen, Z.; Scherf, U.; Koch, N.; Facchetti, A.; et al. Influence of Aggregation on the Performance of All-Polymer Solar Cells Containing Low-Bandgap Naphthalenediimide Copolymers. *Adv. Energy Mater.* **2012**, *2* (3), 369–380. https://doi.org/10.1002/aenm.201100601.
(23) Kang, H.; Kim, K.-H.; Choi, J.; Lee, C.; Kim, B. J. High-Performance All-Polymer Solar Cells Based on Face-On Stacked Polymer Blends with Low Interfacial Tension. *ACS Macr* **2014**, *3* (10). https://doi.org/10.1021/mz500415a.
(24) Yuan, J.; Xu, Y.; Shi, G.; Ling, X.; Ying, L.; Huang, F.; Lee, T. H.; Woo, H. Y.; Kim, J. Y.; Cao, Y.; et al. Engineering the Morphology *via* Processing Additives in Multiple All-Polymer Solar Cells for Improved Performance. *J. Mater. Chem. A* **2018**, *6* (22), 10421–10432. https://doi.org/10.1039/C8TA03343A.
(25) Jia, P.; Xia, H.; Tang, K.; Zhou, Y. Plasticizers Derived from Biomass Resources: A Short Review. *Polymers*. MDPI AG November 24, 2018, p 1303. https://doi.org/10.3390/polym10121303.
(26) Li, Z.; Xu, X.; Zhang, W.; Meng, X.; Ma, W.; Yartsev, A.; Inganäs, O.; Andersson, M. R.; Janssen, R. A. J.; Wang, E. High Performance All-Polymer Solar Cells by Synergistic Effects of Fine-Tuned Crystallinity and Solvent Annealing. *J. Am. Chem. Soc.* **2016**, *138* (34), 10935–10944. https://doi.org/10.1021/jacs.6b04822.
(27) Mori, D.; Benten, H.; Okada, I.; Ohkita, H.; Ito, S. Highly Efficient Charge-Carrier Generation and Collection in Polymer/Polymer Blend Solar Cells with a Power Conversion Efficiency of 5.7%. *Energy Environ. Sci.* **2014**, *7* (9), 2939. https://doi.org/10.1039/C4EE01326C.
(28) Hammond, M. R.; Kline, R. J.; Herzing, A. A.; Richter, L. J.; Germack, D. S.; Ro, H.-W.; Soles, C. L.; Fischer, D. A.; Xu, T.; Yu, L.; et al. Molecular Order in High-Efficiency Polymer/Fullerene Bulk Heterojunction Solar Cells. *ACS Nano* **2011**, *5* (10), 8248–8257. https://doi.org/10.1021/nn202951e.
(29) Diao, Y.; Zhou, Y.; Kurosawa, T.; Shaw, L.; Wang, C.; Park, S.; Guo, Y.; Reinspach, J. A.; Gu, K.; Gu, X.; et al. Flow-Enhanced Solution Printing of All-Polymer Solar Cells. *Nat. Commun.* **2015**, *6* (1), 7955. https://doi.org/10.1038/ncomms8955.
(30) Rivnay, J.; Mannsfeld, S. C. B.; Miller, C. E.; Salleo, A.; Toney, M. F. Quantitative Determination of Organic Semiconductor Microstructure from the Molecular to Device Scale. *Chem. Rev.* **2012**, *112* (10), 5488–5519. https://doi.org/10.1021/cr3001109.
(31) Baker, J. L.; Jimison, L. H.; Mannsfeld, S.; Volkman, S.; Yin, S.; Subramanian, V.; Salleo, A.; Alivisatos, A. P.; Toney, M. F. Quantification of Thin Film Crystallographic Orientation Using X-Ray Diffraction with an Area Detector. *Langmuir* **2010**, *26* (11), 9146–9151. https://doi.org/10.1021/la904840q.
(32) Rivnay, J.; Toney, M. F.; Zheng, Y.; Kauvar, I. V.; Chen, Z.; Wagner, V.; Facchetti, A.; Salleo, A. Unconventional Face-on Texture and Exceptional in-Plane Order of a High Mobility n-Type Polymer. *Adv. Mater.* **2010**, *22* (39), 4359–4363. https://doi.org/10.1002/adma.201001202.
(33) Schubert, M.; Collins, B. A.; Mangold, H.; Howard, I. A.; Schindler, W.; Vandewal, K.; Roland, S.; Behrends, J.; Kraffert, F.; Steyrleuthner, R.; et al. Correlated Donor/Acceptor Crystal Orientation Controls Photocurrent Generation in All-Polymer Solar Cells. *Adv.*

Funct. Mater. **2014**, *24* (26), 4068–4081. https://doi.org/10.1002/adfm.201304216.
(34) Zhang, L.; Xu, X.; Lin, B.; Zhao, H.; Li, T.; Xin, J.; Bi, Z.; Qiu, G.; Guo, S.; Zhou, K.; et al. Achieving Balanced Crystallinity of Donor and Acceptor by Combining Blade-Coating and Ternary Strategies in Organic Solar Cells. *Adv. Mater.* **2018**, 1805041. https://doi.org/10.1002/adma.201805041.
(35) Naveed, H. B.; Zhou, K.; Ma, W. Interfacial and Bulk Nanostructures Control Loss of Charges in Organic Solar Cells. *Acc. Chem. Res.* **2019**, *52* (10), 2904–2915. https://doi.org/10.1021/acs.accounts.9b00331.
(36) Gu, X.; Reinspach, J.; Worfolk, B. J.; Diao, Y.; Zhou, Y.; Yan, H.; Gu, K.; Mannsfeld, S.; Toney, M. F.; Bao, Z. Compact Roll-to-Roll Coater for in Situ X-Ray Diffraction Characterization of Organic Electronics Printing. *ACS Appl. Mater. Interfaces* **2016**, *8* (3), 1687–1694. https://doi.org/10.1021/acsami.5b09174.
(37) Liu, F.; Ferdous, S.; Schaible, E.; Hexemer, A.; Church, M.; Ding, X.; Wang, C.; Russell, T. P. Fast Printing and In Situ Morphology Observation of Organic Photovoltaics Using Slot-Die Coating. *Adv. Mater.* **2015**, *27* (5), 886–891. https://doi.org/10.1002/adma.201404040.
(38) Wang, G.; Eastham, N. D.; Aldrich, T. J.; Ma, B.; Manley, E. F.; Chen, Z.; Chen, L. X.; de la Cruz, M. O.; Chang, R. P. H.; Melkonyan, F. S.; et al. Photoactive Blend Morphology Engineering through Systematically Tuning Aggregation in All-Polymer Solar Cells. *Adv. Energy Mater.* **2018**, *8* (12), 1702173. https://doi.org/10.1002/aenm.201702173.
(39) Kang, H.; Uddin, M. A.; Lee, C.; Kim, K.-H.; Nguyen, T. L.; Lee, W.; Li, Y.; Wang, C.; Woo, H. Y.; Kim, B. J. Determining the Role of Polymer Molecular Weight for High-Performance All-Polymer Solar Cells: Its Effect on Polymer Aggregation and Phase Separation. **2015**. https://doi.org/10.1021/ja5123182.
(40) Bi, Z.; Naveed, H. B.; Mao, Y.; Yan, H.; Ma, W. Importance of Nucleation during Morphology Evolution of the Blade-Cast PffBT4T-2OD-Based Organic Solar Cells. *Macromolecules* **2018**, *51* (17), 6682–6691. https://doi.org/10.1021/acs.macromol.8b01156.
(41) Doumon, N. Y.; Wang, G.; Qiu, X.; Minnaard, A. J.; Chiechi, R. C.; Koster, L. J. A. 1,8-Diiodooctane Acts as a Photo-Acid in Organic Solar Cells. *Sci. Rep.* **2019**, *9* (1), 1–14. https://doi.org/10.1038/s41598-019-40948-1.
(42) Jacobs, I. E.; Wang, F.; Bedolla Valdez, Z. I.; Ayala Oviedo, A. N.; Bilsky, D. J.; Moulé, A. J. Photoinduced Degradation from Trace 1,8-Diiodooctane in Organic Photovoltaics. *J. Mater. Chem. C* **2018**, *6* (2), 219–225. https://doi.org/10.1039/C7TC04358A.
(43) Sharenko, A.; Treat, N. D.; Love, J. A.; Toney, M. F.; Stingelin, N.; Nguyen, T. Q. Use of a Commercially Available Nucleating Agent to Control the Morphological Development of Solution-Processed Small Molecule Bulk Heterojunction Organic Solar Cells. *J. Mater. Chem. A* **2014**, *2* (38), 15717–15721. https://doi.org/10.1039/c4ta03469d.
(44) Hiszpanski, A. M.; Khlyabich, P. P.; Loo, Y. L. Tuning Kinetic Competitions to Traverse the Rich Structural Space of Organic Semiconductor Thin Films. *MRS Commun.* **2015**, *5* (3), 407–421. https://doi.org/10.1557/mrc.2015.55.

TOC Graphic

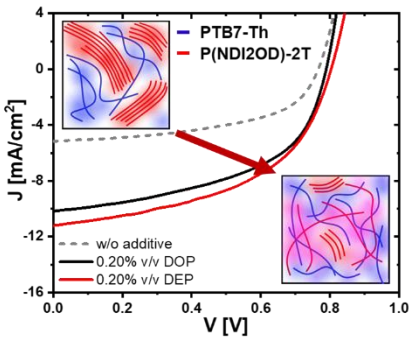

Phthalate additive strategy

- ✓ **Polymer crystallinity control**
- ✓ **High PCE blade-coated all-PSC**
- ✓ **Process transfer to scaleable printing techniques**